Supplementary Information

CONTENTS

I. MODELING.

A. Numerical simulation of the counter-propagating OPO

Defining the rotating frame as

$$H_{rot}/\hbar = \omega_p(b_{cw}^\dagger b_{cw} + b_{ccw}^\dagger b_{ccw}) + \frac{\omega_p}{2}(a_{cw}^\dagger a_{cw} + a_{ccw}^\dagger a_{ccw}), \tag{S1}$$

where $a_{cw,ccw}$ are annihilation operators for half-harmonic signal and idler modes, $b_{cw,ccw}$ are those for pump modes, and ω_p is pump laser frequency. The Hamiltonian of the counter-propagating OPO in this frame can be written as

$$\begin{aligned} H/\hbar = &\delta_a(a_{cw}^\dagger a_{cw} + a_{ccw}^\dagger a_{ccw}) + \delta_b(b_{cw}^\dagger b_{cw} + b_{ccw}^\dagger b_{ccw}) \\ &+ [g_2 a_{cw}^\dagger a_{ccw}^\dagger (b_{cw} + b_{ccw}) + h.c.] \\ &+ (g_{sa} a_{cw}^\dagger a_{ccw} + g_{sb} b_{cw}^\dagger b_{ccw} + h.c.) \\ &+ \varepsilon_P(b_{ccw}^\dagger + h.c.), \end{aligned} \tag{S2}$$

Where pump is injected into the mode b_{ccw}. Defining initial resonance mismatch factor as $\Delta = 2\omega_a - \omega_b$, where $\omega_a = \omega_{a,cw} = \omega_{a,ccw}$ is the unperturbed cavity resonance for half-harmonic modes and $\omega_b = \omega_{b,cw} = \omega_{b,ccw}$ is that for pump modes. The detuning for half-harmonic modes can be expressed by $\delta_a = \omega_a - \omega_p/2 = \frac{\Delta+\delta_b}{2}$. Here, g_2 represents the second-order nonlinear coupling rate, g_{sa} and g_{sb} denote the back scattering coupling rate for half-harmonic and pump modes, and $\varepsilon_P = \sqrt{\frac{2\kappa_{b,ex}P_{in}}{\hbar\omega_b}}$ is pump strength.

The coupling mode equations are thus calculated via $\frac{da}{dt} = -i[a, H/\hbar]$ to be

$$\begin{aligned} \frac{da_{cw}}{dt} &= -i\delta_a a_{cw} - \kappa_a a_{cw} - ig_2(b_{cw}a_{ccw}^\dagger + b_{ccw}a_{ccw}^\dagger) - ig_{sa}a_{ccw} \\ \frac{da_{ccw}}{dt} &= -i\delta_a a_{ccw} - \kappa_a a_{ccw} - ig_2(b_{cw}a_{cw}^\dagger + b_{ccw}a_{cw}^\dagger) - ig_{sa}a_{cw} \\ \frac{db_{cw}}{dt} &= -i\delta_b b_{cw} - \kappa_b b_{cw} - ig_2 a_{cw}a_{ccw} - ig_{sb}b_{ccw} \\ \frac{db_{ccw}}{dt} &= -i\delta_b b_{ccw} - \kappa_b b_{ccw} - ig_2 a_{cw}a_{ccw} - ig_{sb}b_{cw} - i\varepsilon_P. \end{aligned} \tag{S3}$$

The simulation in the main manuscript for Fig.2 and Fig.5 are performed by numerically solving the above CMEs. Simulation parameters for Fig.2 are: $\Delta = 0$, $g_2 = 0.2\,\mathrm{MHz}$, P_{in}=5 mW, κ_b=641 MHz, $\kappa_{cw} = \kappa_{ccw}$=192 MHz, assuming critical coupling for all the modes so $\kappa_{in} = \kappa_{ex}$.

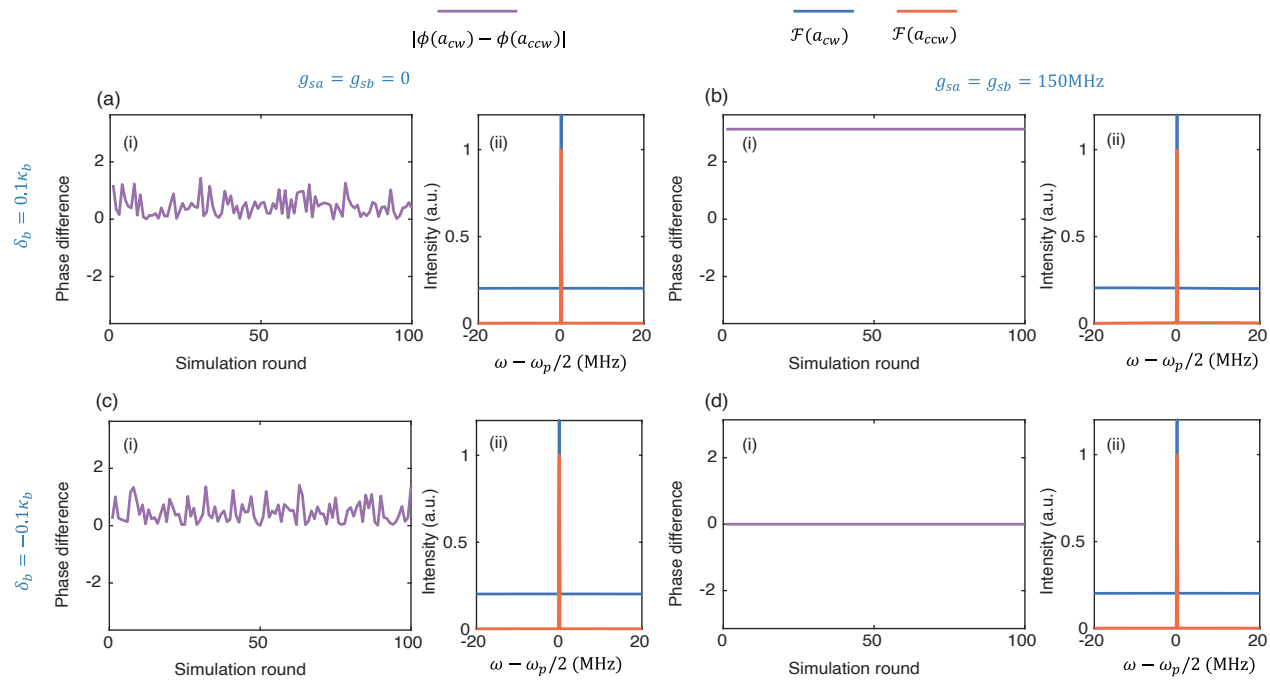

Extended Fig. S1 – **Influence of backscattering on phase locking** **a,** (i) The phase difference betweem signal (a_{cw}) and idler (a_{ccw}) and (ii) the frequency spectrum for them when linear coupling $g_{sa} = g_{sb} = 0$ and pump detuning is $\delta_b = 0.1\kappa_b$. **b,** The same plots when $g_{sa} = g_{sb} = 150$MHz and $\delta_b = 0.1\kappa_b$. **c,** The same plots when $g_{sa} = g_{sb} = 0$ and $\delta_b = -0.1\kappa_b$. **d,** The same plots when $g_{sa} = g_{sb} = 150$MHz and $\delta_b = -0.1\kappa_b$. Other parameters used in simulation: $\Delta = 0$, g_2 =0.2MHz, P_{in} = 5mW, κ_b=641MHz, κ_a=192MHz.

B. Counter-propagating OPO without backscattering coupling

When $g_{sa} = g_{sb} = 0$, the OPO is essentially a nondegenerate OPO happening between pump mode b_{ccw} and signal mode a_{cw} and idler mode a_{ccw}, the phases between the three lasing signals satisfy $\phi_s + \phi_i + \pi/2 = \phi_p + 2n\pi$, where $n = 0, 1, 2...$. This constraint cannot uniquely determine the value for ϕ_s and ϕ_i. If the system is reciprocal so that modes a_{cw} and a_{ccw} share the same physical properties ($\delta_{a,cw} = \delta_{a,ccw}, \kappa_{a,cw} = \kappa_{a,ccw}$), then the generated signal and idler will happen to be frequency-degenerate but still not phase-locked. In order to demonstrate that counter-propagating phase matching itself gives only frequency degeneracy without phase locking, we solve the above CMEs by setting $g_{sa} = g_{sb} = 0$, the simulated phase difference between a_{cw} and a_{ccw} are presented in Fig. S1 (a-i), the variations of $|\phi_{cw} - \phi_{ccw}|$ in different simulation rounds clealy demonstrate their phase-unlocking. The frequency spectrum shown in Fig. S1 (a-ii) indicates that their frequency are locked to the degeneracy point $\omega_p/2$.

As a comparison, the phase differences between signal and idler when turning on the linear coupling term show a deterministic value over different simulation rounds, which is either π when $\delta_b = 0.1\kappa_b$ (Fig. S1 b) or 0 when $\delta_b = -0.1\kappa_b$ (Fig. S1 d).

C. Theoretical analysis of the counter-propagating OPO

Defining hybridized mode basis as $a_1 = \frac{a_{cw}+a_{ccw}}{\sqrt{2}}, a_2 = \frac{a_{cw}-a_{ccw}}{\sqrt{2}}, b_1 = \frac{b_{cw}+b_{ccw}}{\sqrt{2}}, b_2 = \frac{b_{cw}-b_{ccw}}{\sqrt{2}}$, the Hamiltonian can be rewritten in the hybridized mode basis as

$$\begin{aligned} H_{hybri}/\hbar = &(\delta_a + g_{sa})a_1^\dagger a_1 + (\delta_a - g_{sa})a_2^\dagger a_2 + (\delta_b + g_{sb})b_1^\dagger b_1 + (\delta_b - g_{sb})b_2^\dagger b_2 \\ &+ \frac{\sqrt{2}g_2}{2}[(a_1^{\dagger 2} - a_2^{\dagger 2})b_1 + h.c.] \\ &+ \frac{\sqrt{2}\varepsilon_P}{2}(b_1^\dagger - b_2^\dagger + h.c.). \end{aligned} \tag{S4}$$

The nonlinear interaction term in this Hamiltonian reveals two key insights, 1. only the symmetric hybridized pump mode b_1 will participate in the $\chi^{(2)}$ interaction, whereas the hybridized pump mode b_2 serves as additional pump power dissipation channel. 2. inclusion of linear coupling leads to the formation of two distinct degenerate OPO states, one occurring between the modes b_1 and a_1, another occurring between b_1 and a_2. The coupling mode equations (CMEs) are thus calculated via $\frac{da}{dt} = -i[a, H_{hybri}/\hbar]$ to be

$$\begin{aligned}
\frac{da_1}{dt} &= -i(\delta_a + g_{sa})a_1 - \kappa_{a1}a_1 - i\sqrt{2}g_2 a_1^\dagger b_1 \\
\frac{da_2}{dt} &= -i(\delta_a - g_{sa})a_2 - \kappa_{a2}a_2 + i\sqrt{2}g_2 a_2^\dagger b_1 \\
\frac{db_1}{dt} &= -i(\delta_b + g_{sb})b_1 - \kappa_{b1}b_1 - i\frac{g_2}{\sqrt{2}}(a_1^2 - a_2^2) - i\frac{\varepsilon_P}{\sqrt{2}} \\
\frac{db_2}{dt} &= -i(\delta_b - g_{sb})b_2 - \kappa_{b2}b_2 + i\frac{\varepsilon_P}{\sqrt{2}}.
\end{aligned} \tag{S5}$$

The above CMEs have two sets of steady-state solution, i.e. $a_2 = 0, \frac{da_1}{dt} = 0, \frac{db_1}{dt} = 0$ and $a_1 = 0, \frac{da_2}{dt} = 0, \frac{db_1}{dt} = 0$. Analytical analysis for the system can be given based on certain simplifications and assumptions. The thresholds for hybridized OPOs can be analytically solved and compared. Consider the steady OPO emission between a_1 and b_1 when $a_2 = 0$, then we have

$$-i\delta_{a1}a_1 - \kappa_{a1}a_1 - i\sqrt{2}g_2 a_1^\dagger b_1 = 0 \tag{S6}$$

$$-i\delta_{b1}b_1 - \kappa_{b1}b_1 - i\frac{g_2}{\sqrt{2}}a_1^2 - i\frac{\varepsilon_P}{\sqrt{2}} = 0, \tag{S7}$$

where $\delta_{a1} = \delta_a + g_{sa} = \frac{\Delta+\delta_b}{2} + g_{sa}$, $\delta_{b1} = \delta_b + g_{sb}$. Therefore, when OPO reaches steady-state, $b_1 = \frac{-i\delta_{a1}-\kappa_{a1}}{i\sqrt{2}g_2}\frac{a_1}{a_1^\dagger} = \frac{-i\delta_{a1}-\kappa_{a1}}{i\sqrt{2}g_2}e^{i2\phi_1}$, assuming $a_1 = |a_1|e^{i\phi_1}$. Substituting this expression for b_1 into Eq. S7, we have

$$(-i\delta_{b1} - \kappa_{b1}) \cdot \frac{-i\delta_{a1} - \kappa_{a1}}{ig_2} - ig_2|a_1|^2 = i\varepsilon_P e^{-i2\phi_1}. \tag{S8}$$

Separating the real and imaginary part of Eq. S8 gives

$$\kappa_{a1}\kappa_{b1} - \delta_{a1}\delta_{b1} + g_2^2|a_1|^2 = -g_2\varepsilon_P \cos(2\phi_1), \tag{S9}$$

$$\delta_{a1}\kappa_{b1} + \delta_{b1}\kappa_{a1} = g_2\varepsilon_P \sin(2\phi_1). \tag{S10}$$

Since $|a_1|^2 = \frac{\varepsilon_P}{g_2} \cdot \sqrt{1 - \frac{(\delta_{a1}\kappa_{b1}+\delta_{b1}\kappa_{a1})^2}{g_2^2\varepsilon_P^2}} - \frac{\kappa_{a1}\kappa_{b1}-\delta_{a1}\delta_{b1}}{g_2^2} + \geq 0$, the resulted ε_P should satisfy

$$\varepsilon_P^2 \geq \frac{(\kappa_{a1}\kappa_{b1} - \delta_{a1}\delta_{b1})^2 + (\delta_{a1}\kappa_{b1} + \delta_{b1}\kappa_{a1})^2}{g_2^2}. \tag{S11}$$

Hence the threshold pump powers for the hybridized OPOs are

$$P_{th,i} = \frac{(\kappa_{ai}\kappa_{b1} - \delta_{ai}\delta_{b1})^2 + (\delta_{ai}\kappa_{b1} + \delta_{b1}\kappa_{ai})^2}{g_2^2} \cdot \frac{\hbar\omega_p}{2\kappa_{b1,ex}}. \tag{S12}$$

The subscript $i \in \{1, 2\}$ denotes the indices for the symmetric and asymmetric hybridized half-harmonic modes, respectively. The phase transition occurs when the threshold pump powers are equal, i.e., $P_{th,1} = P_{th,2}$. In the case where the two hybridized modes share the same dissipation rate $\kappa_{a1} = \kappa_{a2} = \kappa_a$ and the liner coupling rates are the same $g_{sa} = g_{sb} = g_c$, the phase transition point is reached when the pump detuning compensates for the initial resonance mismatch, namely, when $\delta_b = -\Delta$, thus $\delta_{a1,a2} = \pm g_c$, $\delta_{b1} = g_c - \Delta$. At this point, the co-shared threshold power can be simplified into:

$$P_{th,c} = \frac{\hbar\omega_p}{2\kappa_{ex,b1}} \cdot \frac{[(g_c - \Delta)^2 + \kappa_{b1}^2] \cdot (\kappa_a^2 + g_c^2)}{g_2^2}. \tag{S13}$$

The occurrence of dual OPO states and associated phase transition point is guaranteed when the applied pump power surpass this co-shared threshold power. A larger linear coupling rate g_c will elevate the required power for dual OPO states. The permissible range of linear coupling for the coexistence of dual OPO states is depicted in Fig. S2(a).

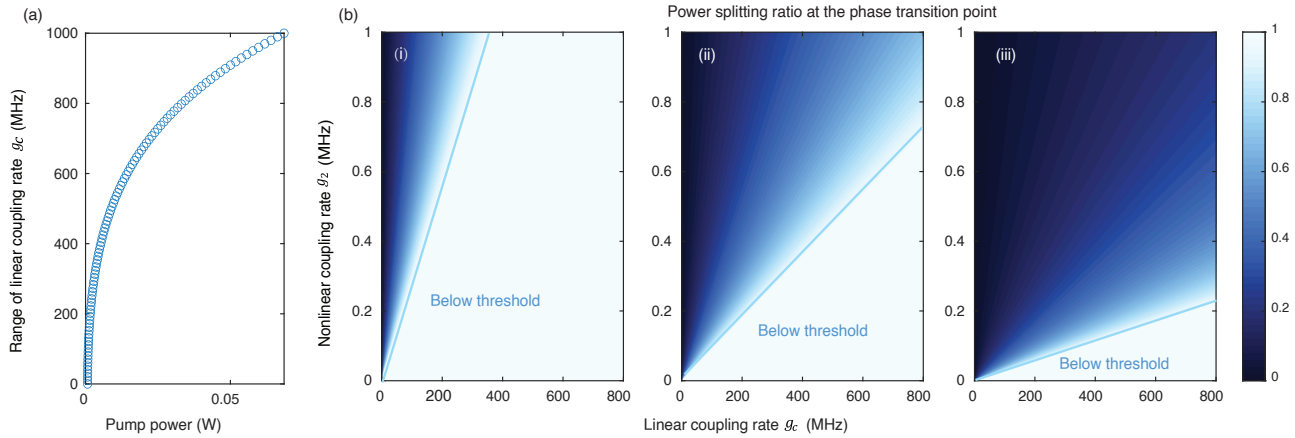

Extended Fig. S2 – **Theoretical calculation results a,** (i) The permissible linear coupling range for coexistence of dual degenerate OPO states for different pump power. **b,** The power splitting ratio under different linear and nonlinear coupling rates. Panels (i-iii) depict the situation when applied pump power is 0.1, 1, 10 mW, respectively. Other parameters used here are: $\Delta = 0$, g_2 =0.2MHz, P_{in} = 5mW, κ_{b1}=641MHz, κ_a=192MHz.

At the phase transition points, both hybridized OPOs are lasing simultaneously, the resulted output signal a_{cw} and idler a_{ccw} are thus an interference between the lased OPOs. The photon-number splitting ratio R are calculated via

$$R = \frac{|a_{cw}|^2 - |a_{ccw}|^2}{2|a_1||a_2|} = \cos(\phi_1 - \phi_2),$$

where $\phi_i = \frac{1}{2}\arcsin(\frac{\delta_{ai}\kappa_{b1} - \Delta\kappa_{ai}}{g_2\varepsilon_P})$, $\delta_{ai} = (-1)^{i-1}g_{sa}$ $i \in \{1, 2\}$. The splitting ratio basically increases as linear coupling rate g_{sa} increases while a larger $\chi^{(2)}$ nonlinear coupling rate and a more intense pump lower down the ratio, as illustrated by Fig. S2(b).

II. MEASUREMENT

A. Experiment setup for OPO measurement

The pump laser is a custom-built amplified pulsed laser. A continuous wave (CW) seed laser at 1550 nm is shaped into pulses using an intensity electro-optic modulator (EOM) controlled by an arbitrary waveform generator (AWG). The AWG outputs voltages V_{high} and V_{low} to switch the EOM between its on and off states. The pulses are then amplified using a two-stage EDFA setup, with a 1 nm bandwidth filter placed between the EDFAs to remove background noise from the first stage and enhance the pulse extinction ratio. The amplified infrared pulses are subsequently frequency-doubled to the visible range using a commercial PPLN crystal [Fig. S4(a)]. A visible photon detector measures the average power of the pulse P_{on}, and the peak power is calculated using $(P_{\text{on}} - P_{\text{off}})/f_{\text{rep}}W$, where P_{off} represents the optical power when AWG output is DC off state. In our experiment, the repetition rate f_{rep} and pulse duration W are set to be 5 KHz and 15 ns for the measurements in Fig.4 in the main manuscript.

For OPO generation, the visible pump laser is injected through the 780 nm port of the left wavelength-division multiplexer (WDM), while the generated signal is collected from the 1550 nm port on the same side. A second WDM on the opposite side separates the transmitted pump light and the generated idler. To prevent residual pump light from interfering with the photodetector (PD) response, silicon absorbers with 40 dB attenuation at 780 nm are used. To verify that the signal and idler are generated at degeneracy, a local oscillator, provided by another 1550 nm laser, is split into two paths and mixed with both the signal and idler for simultaneous beat-note detection. The resulting signals are recorded by two fast (12 GHz) photon detectors and analyzed using an electrical spectrum analyzer (ESA) [Fig. S4(b)].

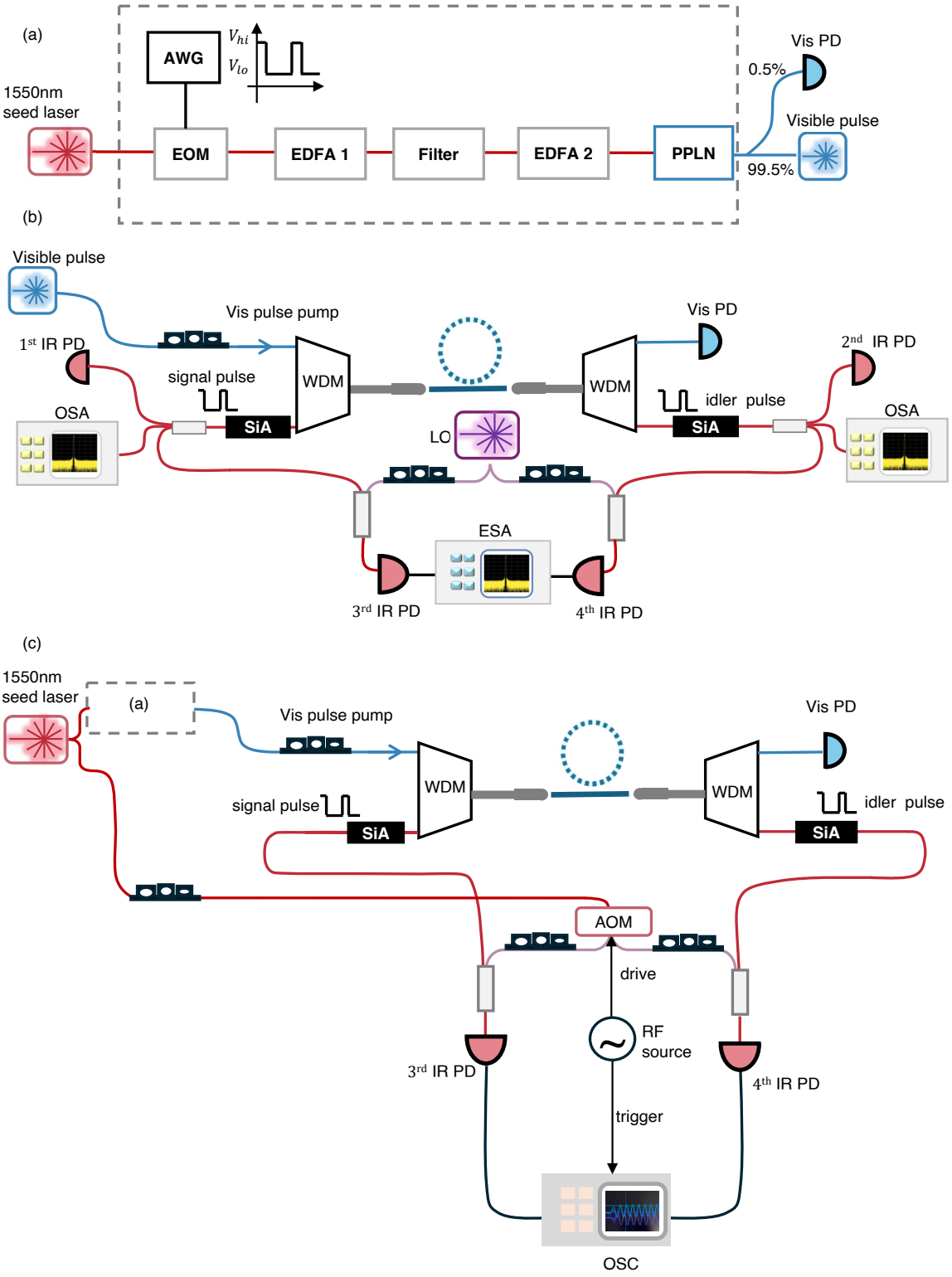

Extended Fig. S3 – **Measurement Setup a,** Schematic of the 780 nm nanosecond pulsed laser system. **b,** Experimental setup for counter-propagating OPO measurement. SiA represents a silicon absorber used to block transmitted or reflected residual 780 nm pump light. The first and second infrared photon detectors are slow, while the third and fourth detectors are high-speed. The local oscillator is another continuous-wave 1550 nm laser with a fixed wavelength. **c,** Experimental setup for phase measurement of the degeneracy-locked OPO. Here, the local oscillator is derived from the same 1550 nm seed laser and frequency-shifted by 300 MHz using an AOM.

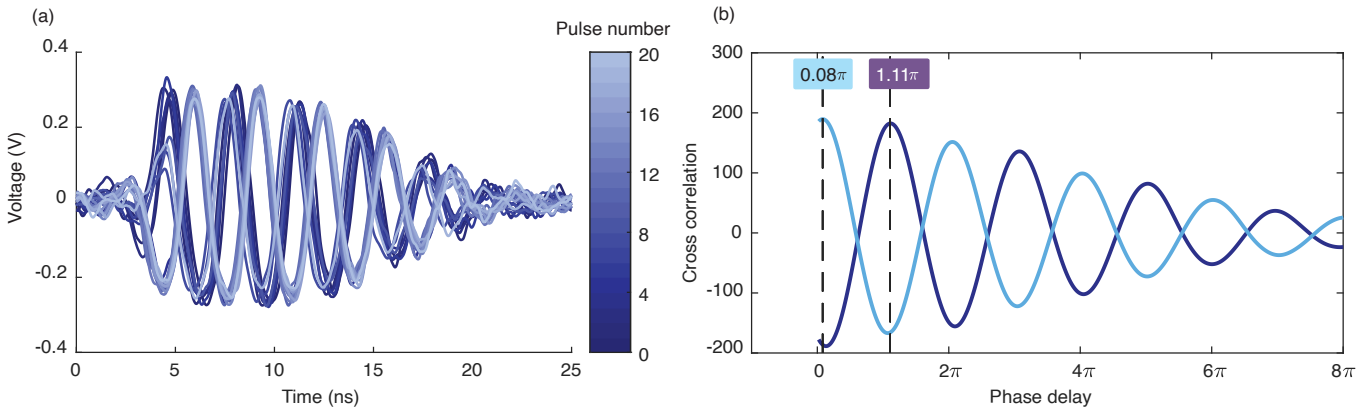

Extended Fig. S4 – **Phase measurement a,** Beat notes of 20 consecutive signal pulses mixed with the AOM-shifted laser. **b,** Cross-correlation of the 4th–5th and 6th–7th beat notes from (a), revealing phase delays of 0.08π and 1.11π, respectively.

B. Degenerate OPO phase measurement

To measure the phase differences between consecutive signal pulses in the degenerate OPO, 10% of the 1550 nm seed laser is extracted and sent to a 300 MHz acousto-optic modulator (AOM), while the remaining 90% follows the optical path shown in Fig. S4(a) to generate the 780 nm pulsed pump.

The AOM-shifted laser is mixed with the generated signal, producing a 300 MHz beat note with a pulsed envelope. The pump repetition rate is set to 100 kHz, with a pulse duration of 50 ns. Since the relative phase between the signal and pump randomly locks to either 0 or π upon each OPO initiation, the phase differences between consecutive signal pulses are also expected to be 0 or π, provided the pump phase remains stable over one pulse period (10 μs). An oscilloscope records the beat notes, and Fig. S4(a) displays 20 overlaid consecutive beat notes, showing 300 MHz oscillations with binary phase relationships.

Phase difference is determined via cross-correlation, with the delay at peak correlation corresponding to the phase changes between successive pulses. Fig. S4(b) presents two example cross-correlation curves, where peak values occur at phase delays of approximately 0 or π. The distribution centered around 0 and π in Fig. 4(d) of the main manuscript is attributed to pump phase variations during a single pulse period.

The same data acquisition and analysis procedure is applied to idler pulses.

C. Symmetric second-harmonic generation

To ignite counter-propagating OPO, the initial resonance mismatch Δ should be optimized, ideally close to zero. Thus, the preliminary resonance alignment between the pump mode (ω_b) and the signal/idler mode (ω_a) is achieved using a threshold-less symmetric second-harmonic generation (SSHG) measurement. In this process, continuous wave 1550 nm light is injected from both ends of the device, and symmetric SHG outputs are simultaneously monitored. The chip temperature is adjusted using a heater beneath the chip holder, with the optimal operating temperature determined by the peak SHG output. The 3-dB temperature bandwidth for SSHG is approximately 0.37°C, as shown in Fig. S5(a).

Following the initial alignment procedure, we calibrated the nonlinear coupling rate g_2 through SSHG power measurements in the pump undepleted regime. By fitting the on-chip left-propagating SSHG power as a function of on-chip pump power, we determined an SHG efficiency of $P_{SHG}/P_p^2 = 19790\%/\mathrm{W}$ (Fig. S5(b)), where P_{SHG} and P_p represent the one-sided SHG power and one-sided pump power, respectively. The theoretical expression for the SHG conversion efficiency is given by:

$$\frac{P_{SHG}}{P_p^2} = \frac{g_2^2\omega_b}{\hbar\omega_p^2} \cdot \frac{2\kappa_{ex,b}}{\delta_b^2+\kappa_b^2} \cdot \left(\frac{2\kappa_{ex,a}}{\delta_a^2+\kappa_a^2}\right)^2, \tag{S14}$$

where g_2 is the nonlinear coupling rate, κ_a, $\kappa_{ex,a}$, κ_b, and $\kappa_{ex,b}$ are the external and total coupling rates for mode a and b, δ_a and δ_b are the mode detunings. By substituting the experimentally fitted values for $\kappa_{ex,a}$, κ_a, $\kappa_{ex,b}$, and κ_b

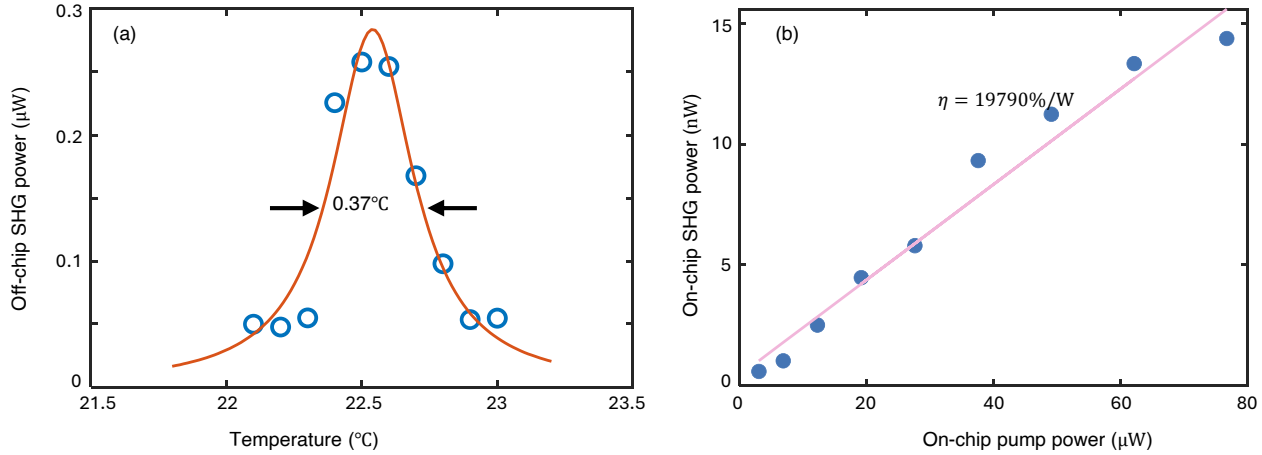

Extended Fig. S5 – **Symmetric SHG measurement a,** Symmetric SHG output power as temperature varies. The full-width at half-maximum window is fitted to be 0.37 ° **b,** Symmetric SHG conversion efficiency at pump undepleted regime.

into Eq. S14, and assuming an ideal dual-resonance condition where $\delta_a = \delta_b = 0$, we calculate the coupling rate g_2 to be 0.2 MHz. This result is based on experimentally measured quality factors of $Q_{a,in} = 7.75 \times 10^5$, $Q_{a,ex} = 5.04 \times 10^6$, $Q_{b,in} = 6.10 \times 10^5$, and $Q_{b,ex} = 8.22 \times 10^6$. The resulted theoretical threshold power for OPO is thus calculated to be 1.4 mW according to Eq. S13, which is consistent in order of magnitude with the experimentally measured value. The nonlinear coupling rate can be further enhanced by utilizing d_{33} for conversion from the 780 nm TM00 mode to the 1560 nm TM00 mode. However, the current device exhibits a lower quality factor for the TM00 mode compared to the TE00 mode, requiring further optimization to improve quality factors for efficient TM00-TM00 conversion.